IEEE Journal of Biomedical and Health Informatics, Available online 12 February 2025
DOI:10.1109/jbhi.2025.3541004

AI-assisted In silico Trial for the Optimization of Osmotherapy after Ischaemic Stroke

Xi Chen, Lei Lu, Tamás I. Józsa, Jiandong Zhou, David A. Clifton, Stephen J. Payne

***Abstract*—Over the past few decades, osmotherapy has commonly been employed to reduce intracranial pressure in post-stroke oedema. However, evaluating the effectiveness of osmotherapy has been challenging due to the difficulties in clinical intracranial pressure measurement. As a result, there are no established guidelines regarding the selection of administration protocol parameters. Considering that the infusion of osmotic agents can also give rise to various side effects, the effectiveness of osmotherapy has remained a subject of debate. In previous studies, we proposed the first mathematical model for the investigation of osmotherapy and validated the model with clinical intracranial pressure data. The physiological parameters vary among patients and such variations can result in the failure of osmotherapy. Here, we propose an AI-assisted in silico trial for further investigation of the optimisation of administration protocols. The proposed deep neural network predicts intracranial pressure evolution over osmotherapy episodes. The effects of the parameters and the choice of dose of osmotic agents are investigated using the model. In addition, clinical stratifications of patients are related to a brain model for the first time for the optimisation of treatment of different patient groups. This provides an alternative approach to tackle clinical challenges with in silico trials supported by both mathematical/physical laws and patient-specific biomedical information.**

***Index Terms*—Osmotherapy, Cerebral oedema, Brain ischaemic stroke, Deep neural network, Finite Element Method.**

I. Introduction

A continuous and sufficient blood supply to the human brain is crucial for cerebral metabolism and proper brain functioning. However, blood vessel blockage during an ischemic stroke can lower cerebral blood flow and disrupt cerebral metabolism, therefore damaging the blood-brain barrier (BBB) and increasing BBB permeability [1, 2]. In clinical settings, reperfusion therapy has been employed to restore blood perfusion to the occluded brain and elevate blood perfusion. As a result, blood components can leak into the interstitial space through damaged BBB (Fig. 1) and give rise to brain oedema which is marked by elevated intracranial pressure (ICP), tissue swelling, increased tissue stress and strain [3]. Symptoms of an elevated ICP include headache, nausea, vomiting, and unconsciousness. An ICP of more than 25 mmHg is usually considered life-threatening and requires urgent medical treatment [4]. Over the past few decades, osmotherapy has been used extensively to lower ICP down to the typical range of 5 to 15 mmHg [4, 5].

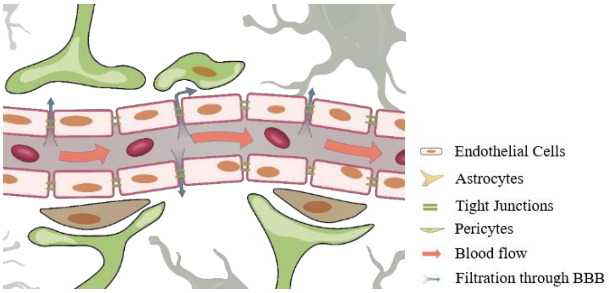

Figure 1: Illustration of blood leaking from a capillary vessel segment. Oedema formation is associated with blood leaving the lumen through the damaged blood brain barrier, filling the interstitial space, and thus causing tissue swelling.

Mannitol, hypertonic saline, sorbitol, and glycerol are the four types of osmotic agents that are now used for treatment, with hypertonic saline becoming increasingly popular in recent years [6, 7]. Hypertonic saline reduces the amount of interstitial fluid and relieves oedema by producing an osmotic pressure gradient that drives excessive fluid from the interstitial space into the intravascular space. Although osmotic agent has a number of benefits, its side-effects have also been reported in previous studies [7, 8]. One issue is that hyperchloremic acidosis may result from the elevated Cl^- level

Stephen J. Payne is supported by a Yushan Fellowship from the Ministry of Education, Taiwan (111V1004-2). David A. Clifton is supported by the Pandemic Sciences Institute at the University of Oxford; the National Institute for Health Research (NIHR) Oxford Biomedical Research Centre (BRC); an NIHR Research Professorship; a Royal Academy of Engineering Research Chair; and the InnoHK Hong Kong Centre for Centre for Cerebro-cardiovascular Engineering (COCHE). (Xi Chen and Lei Lu contributed equally.) (Corresponding authors: David A. Clifton; Stephen J. Payne)

Xi Chen, Lei Lu and David Clifton are with the Institute of Biomedical Engineering, Department of Engineering Science, University of Oxford, Oxford, United Kingdom (e-mail: xi.chen2@st-hildas.ox.ac.uk, lei.lu@eng.ox.ac.uk, david.clifton@eng.ox.ac.uk)

Lei Lu is with the School of Life Course and Population Sciences, King's College London, London, SE1 1UL, UK.

Tamás I. Józsa is with the School of Aerospace, Transport and Manufacturing Cranfield University, Cranfield, United Kingdom (e-mail: tamas.jozsa@cranfield.ac.uk)

Jiandong Zhou is with the Department of School of Public Health, Li Ka Shing Faculty of Medicine, The University of Hong Kong, Hong Kong, China; Department of Family Medicine and Primary Care, Li Ka Shing Faculty of Medicine, The University of Hong Kong, Hong Kong, China; Department of Pharmacology and Pharmacy, The University of Hong Kong, Hong Kong, China.

David Clifton is with the Oxford Suzhou Centre for Advanced Research, University of Oxford, Suzhou Industrial Park, Suzhou, 215123, Jiangsu, China.

Stephen J. Payne is with the Institute of Applied Mechanics, National Taiwan University, Roosevelt Road, Da'an Dist., Taipei City 106, Taiwan (e-mail: stephenpayne@ntu.edu.tw).

Published by IEEE. This is the Author Accepted Manuscript issued with: Creative Commons Attribution License (CC:BY 4.0).
The final published version (version of record) is available online at DOI:10.1109/jbhi.2025.3541004. Please refer to any applicable publisher terms of use.

in hypertonic saline [9]. Furthermore, it has been noted that higher than 160 mmol/L concentrations of NaCl can worsen patient outcomes and aggravate damage to the blood-brain barrier [9, 10]. Therefore, it is essential to balance between achieving an optimised ICP drop and controlling the side-effects. Although osmotherapy outcomes have been investigated in multiple studies [11–13], an optimal administration protocol for hypertonic saline infusion has remained controversial. Patient heterogeneity has been postulated as the cause of the differences in previous investigations [2].

In this study, we aim to tackle the issue by using novel simulation tools that are jointly supported by bioinformation and biophysical laws. The model further develops the repository of the In Silico Clinical Trials for the Treatment of Acute Ischaemic Stroke (INSIST) project [14, 15]. The objective is to incorporate AI-assisted in silico osmotherapy trial into the existing Finite Element (FE) model and explore treatment protocols that are optimal in reducing ICP. The deep learning model can incorporate statistics and therefore establish a connection between patient characteristics and low information-noise ratio clinical data using an FE model based on mathematical and mechanical theories. Once a well-founded model has been obtained, it can enhance the precision of resource-intensive clinical studies, consequently reducing the enormous associated costs. Drawing inspiration from recent investigations on brain modelling [16-20], recent AI applications in biomedical studies [21-23], and the application of AI in the field of engineering [24, 25], a novel AI-assisted in silico trial for the investigation of osmotherapy is thus proposed here.

Here, we present the prediction of the ICP evolution using deep neural network (DNN) model during osmotherapy episodes on a quasi-population level. The paper comprises following sections: (1) the FE model and the training and testing of the neural network will be presented; (2) the effects of physiological parameters on the main features of the osmotherapy will be investigated; (3) the effectiveness of the osmotherapy will be evaluated using two criteria and the effects of different physiological parameters will be presented; (4) customised doses of osmotic agents will be proposed for different levels of BBB damage and age groups.

II. Methods

The model consists of two components, including the FE model and the artificial neural network. The FE models are utilised to generate ICP data and the workflow comprises three FE models for blood perfusion, oedema, and osmotherapy simulations, respectively. After in silico trials, the DNN model is trained using the ICP data and employed for the inference of massive ICP data of virtual patient groups.

A. Perfusion Model

1) Governing Equations: In blood perfusion simulation, the brain is considered a porous medium with three compartments representing the arteriole, venule, and capillary blood, respectively [18, 26, 27]. The pial surface is subdivided into perfusion regions and perfusion in stroke scenarios can be obtained by occluding perfusion territories (Fig. 2a) and compared with healthy perfusion. The governing equations of the three-compartment perfusion model are taken directly from our previous studies:

$$\nabla \cdot (\boldsymbol{K}_a \nabla p_a) = -\omega_{ac} \cdot (p_a - p_c), \quad (1)$$

$$\nabla \cdot (\boldsymbol{K}_c \nabla p_c) = \omega_{ac} \cdot (p_a - p_c) - \omega_{cv} \cdot (p_c - p_v), \quad (2)$$

$$\nabla \cdot (\boldsymbol{K}_v \nabla p_v) = \omega_{cv} \cdot (p_c - p_v), \quad (3)$$

where p_a, p_c and p_v are the blood pressures in the arteriole, capillary, and venule compartments respectively. $\boldsymbol{K_i}$ is the permeability tensor of compartment i, where the capillary tensor field can be replaced with the K_c scalar field.

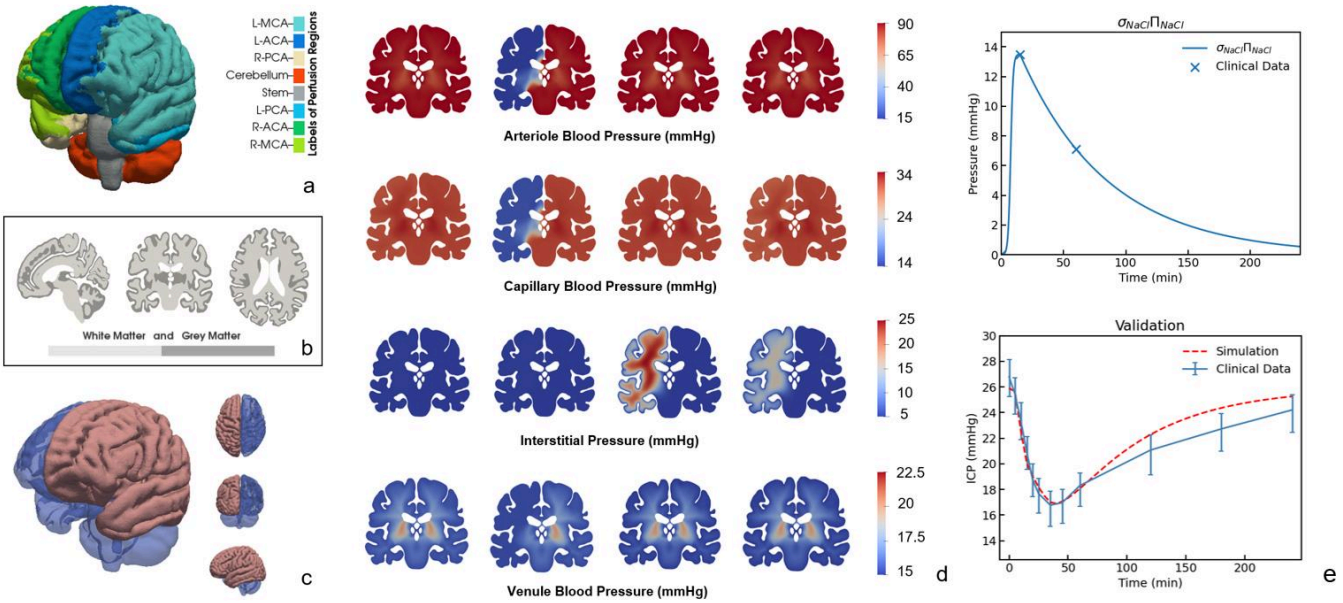

Figure 2: (a) Subdivided perfusion regions on the brain pial surface, where L-PCA, L-MCA, L-ACA and R-PCA, R-MCA, R-ACA denote the

posterior, middle and anterior cerebral arteries on the left and right hemisphere, respectively. Blood flow through any combination of the perfusion territories can be blocked to obtain an occluded blood perfusion map. (b) White and grey matter in the brain model. (c) Left hemisphere oedema volume (red) generated using the perfusion model. (d) blood pressure and interstitial pressure along the coronal plane, from left to right: healthy, stroke, oedema, and osmotherapy. (e) Comparison of the model with clinical osmotic pressure and ICP data, adjusted from [26]

Fluid transfer coefficient between compartments i and j is denoted by ω_{ij}. As flow parameters can be different brain subdomains (Fig. 2b), ω_{ij} in white and grey matter are thus represented by ω_{ac}^{w}, ω_{ac}^{g} and ω_{cv}^{w}, ω_{cv}^{g} in the model.

2) Boundary Conditions: Blood flows into the human brain through arterioles and leaves the brain through venules at the pial surface. Hence, blood flow is non-zero only at the pial surface of the arteriole and venule compartments. In the model, a 90mmHg arteriole blood pressure and a 15mmHg venule pressure are given on the pial surfaces. As demonstrated in [28], each artery is found to supply a certain perfusion region (illustrated in Fig. 2a). In the occluded scenario, blood flow through the arterial perfusion territory of an occluded arteries is set to zero-flux boundary, whereas blood pressure in other regions is assumed to remain unchanged. The boundary conditions of the perfusion model can be summarised in Table 1.

TABLE 1
BOUNDARY CONDITIONS FOR THE PERFUSION MODEL. $\boldsymbol{n}$ is the outward directed normal unit vector of the boundary region.

	Cortical Surface	Ventricle Surface
Arteriole Blood	$p_a = 90$ mmHg (non-occluded regions) $\boldsymbol{K}_a \nabla p_a \cdot \boldsymbol{n} = 0$ (occluded region)	$\boldsymbol{K}_a \nabla p_a \cdot \boldsymbol{n} = 0$
Capillary Blood	$K_c \nabla p_c = 0$	$K_c \nabla p_c \cdot \boldsymbol{n} = 0$
Venule Blood	$p_v = 15$ mmHg	$\boldsymbol{K}_v \nabla p_v \cdot \boldsymbol{n} = 0$

B. Oedema and Osmotherapy Model

1) Governing Equations: The exchange between blood components and the interstitial fluid can be neglected in healthy BBB. However, in the context of a damaged brain, an extra compartment is necessary for interstitial fluid in both the oedema and osmotherapy models to simulate the ICP change. Furthermore, to model ICP evolution in oedema and osmotherapy, time-dependent terms are introduced to the governing equations:

$$c_w \frac{\partial p_w}{\partial t} = \nabla \cdot (K_w \nabla p_w) + S_{cw} \ , \tag{4}$$

$$c_b \frac{\partial p_a}{\partial t} = \nabla \cdot (\boldsymbol{K_a} \nabla p_a) - \omega_{ac} \cdot (p_a - p_c) \ , \tag{5}$$

$$c_b \frac{\partial p_c}{\partial t} = \nabla \cdot (K_c \nabla p_c) + \omega_{ac} \cdot (p_a - p_c) - \omega_{cv} \cdot (p_c - p_v) - S_{cw} \tag{6}$$

$$c_b \frac{\partial p_v}{\partial t} = \nabla \cdot (\boldsymbol{K_v} \nabla p_v) + \omega_{cv} \cdot (p_c - p_v) \ , \tag{7}$$

where c_w is the storage factors of the interstitial fluid and c_b, the storage factors of the blood compartments, is assumed to be the same for arteriole, capillary and venule compartments. The pressure of interstitial fluid and the hydraulic conductivity of interstitial space are denoted by p_w and K_w. ICP is assumed to be equal to p_w. The S_{cw} denotes the leakage rate from the capillary network into the interstitial space. In Equation 4-7, displacement terms in the poroelastic theory can be neglected, as the pressure is found to vary at a much slower time scale compared to tissue displacement [29]. Here, time scale separation can be used and the S_{cw} is derived in [26] and summarised in Table 2.

TABLE 2
FLUID FILTRATION RATE FOR THE OEDEMA AND OSMOTHERAPY MODEL.

	Oedema	Healthy Tissue
Oedema Model	$S_{cw} = 2n_b \frac{L_p}{R_c}[(p_c - p_w) - \sigma \Pi_c]$	0
Osmotherapy Model	$S_{cw} = 2n_b \frac{L_p}{R_c}[(p_c - p_w) - \sigma \Pi_c - \sigma_{NaCl} \Pi_{NaCl}]$	0

L_p is the permeability of the damaged BBB, σ is the reflection coefficient of the blood plasma, n_b is the volume fraction of blood vessels in a unit volume of brain tissue, R_c is the mean radius of capillary vessel, and Π_c represents the osmotic pressure of the blood plasma before hypertonic saline injection. The term $\sigma_{NaCl}\Pi_{NaCl}$ denotes the increase in osmotic pressure in an osmotherapy episode, where σ_{NaCl} and Π_{NaCl} denote the reflection coefficient and osmotic pressure of the injected saline. Due to the fact that the BBB can be much leakier in the damaged tissue, the fluid transfer can be neglected in healthy BBB. The corresponding simulation results are shown in Fig. 2d. The effective osmotic pressure can be written as:

$$\sigma_{NaCl}\Pi_{NaCl} = \begin{cases} \frac{\Pi_{Max}}{1+e^{15(0.5T_{in}-t)/T_{in}}} & ,0 \le t \le T_{in} \\ \Pi_{Max} \cdot e^{-\dot{D}(t-15)} & ,T_{in} < t \le 240 \text{ min.} \end{cases} \tag{8}$$

where the infusion time T_{in} is fixed to be 15 min, and the decay rate $\dot{D}$ is set to be 0.01424 min^{-1} to match the clinical osmotic pressure data (Fig. 2e) [26, 30]. Π_{Max} is the maximum osmotic pressure during an episode.

2) Boundary Conditions: In post-stroke oedema, reperfusion therapy is performed, therefore it is considered that the blood flow restores and there is no occluded region at the pial surface. Normal range of ICP can range from 5-15 mmHg in healthy adults. In the model, we choose healthy interstitial fluid pressure to be 5 mmHg, and the boundary conditions can thus be summarised in Table 3.

TABLE 3:

BOUNDARY CONDITIONS OF THE OEDEMA AND OSMOTHERAPY MODEL.

	Cortical Surface	Ventricle Surface
Arteriole Blood	$p_a = 90$ mmHg	$K_a \nabla p_a \cdot \boldsymbol{n} = 0$
Capillary Blood	$K_c \nabla p_c \cdot \boldsymbol{n} = 0$	$K_c \nabla p_c \cdot \boldsymbol{n} = 0$
Venule Blood	$p_v = 15$ mmHg	$K_v \nabla p_v \cdot \boldsymbol{n} = 0$
Interstitial Fluid	$p_w = 5$ mmHg	$p_w = 5$ mmHg

C. Design of Deep Neural Network Model

To facilitate the simulation process, we developed a deep neural network (DNN) model to explore the relationship between the parameters and the ICP change. The model has an input of five parameters, including the tissue storage factor c_w, tissue hydraulic conductivity K_w, blood vessel permeability L_p, arterial blood pressure ABP (p_a on cortical surface), and the maximum osmotic pressure Π_{Max}. The parameters L_p, c_w and K_w are varied between 0.5 to 2 times their baseline values, as these are the ranges that can be seen in previous studies [31-34], and the blood pressure ABP is varied between 80 mmHg to 100 mmHg [35]. Meanwhile, the maximum osmotic pressure is 1800 Pa in 10% hypertonic saline injection [30]. In the model, the maximum osmotic pressure is varied between 900-3600 Pa, which corresponds to the concentration (5%-20%) of hypertonic saline injection in the literature [2, 36]. The output is a sequence of 49 data points for the ICP values at different time during an osmotherapy episode.

We tried different architectures for the DNN model design, including the models using dense layers, convolutional layers (Conv), long short-term memory (LSMT) layers, and residual neural network (ResNet). More advanced DNN models, such as transformer-based models [37], and diffusion models [38], have also been powerful tools for the regression prediction of biomedical data. In this study, however, we found that the ResNet neural network is sufficient for the prediction analysis of time series ICP data with a reasonably small loss. Using trial-and-error, we searched for an optimal model with the minimal error for the ICP value estimation. As shown in Fig. 3, the final searched DNN model has six convolutional layers and two ResNet blocks. In the first ResNet block, the convolutional layers have 48 kernels with the size of 3; and in the second ResNet block, the convolutional layers have 64 kernels with the size of 3. Then, a dense layer is used to produce the output for the ICP value estimation. The mean squared error between the ICP value and the estimation, summed over all time points, is used as the loss function. The model was trained for 100 epochs with a batch size of 16 and a learning rate of 0.001. Generally, the best model was identified based on the minimal loss during training.

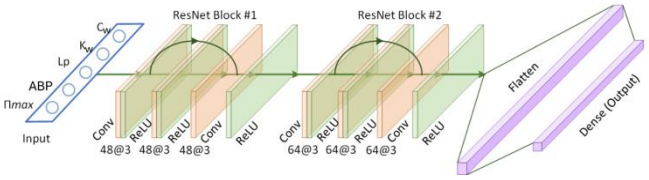

Figure 3: The architecture of DNN model for the ICP value prediction.

D. Model Coupling

The geometry of oedema core is obtained from the perfusion model and used for oedema simulation. The blood perfusion (F) and blood perfusion reduction (ΔF) are defined in Equation 9 and 10, respectively:

$$F = \omega_{ac} \cdot (p_a - p_c) \tag{9}$$

$$\Delta F = \frac{F_{\text{healthy}} - F_{\text{occluded}}}{F_{\text{healthy}}} \times 100\% \ , \tag{10}$$

A blood perfusion reduction of 70% and over has been used in clinical imaging to determine brain damage regions [39, 40] and the threshold is thus utilised to obtain the geometry of oedema lesion in our model (Fig. 2c). In the oedema model, the pressure is iterated over time steps until the ICP (defined to be the spatial maximum of p_w) reaches equilibrium by using the stroke simulation results as the initial condition. Finally, the simulated pressures at the final time step in the oedema model are imported into the osmotherapy model as the initial conditions (Fig. 2d). A full space searching is performed for $\{c_w, \text{ABP}, K_w, L_p, \Pi_{Max}\}$, and 2000 in silico cases were simulated. The data were then used to train and test the artificial neural network, using the process shown in Fig. 4. The model parameter was chosen from the parameter ranges in [2, 31-36] and was validated in two steps. In the first step, the in silico data were compared with 8 patients ICP data who had 22 episodes from [30] and the validation was done by calculating the mean square error between the simulated ICP curve and the clinical data (Fig. 2e). The data generated from the DNN were further validated (second step validation) with previous literature to justify the choice of FE model parameters, as shown in Fig. 4. The parameter sensitivity test is conducted by [26]. The baseline parameters are listed in Table A1.

In the model, the governing equations are solved numerically using Python with a high-performance open-source Finite Element library, FEniCS [41]. The brain mesh used in this study includes 1.4 million tetrahedra and a good mesh convergence has been shown using 0.7 million and 2.8 million tetrahedra meshes. The DNN model is designed with Tensorflow 2.2, Python 3.7.4, and the Nvidia Quadro RTX 6000 is used for the model training. The inference of trained

DNN is found to be 10^8 times faster than the conventional FE simulation method and can thus be used for prediction of osmotherapy in large population.

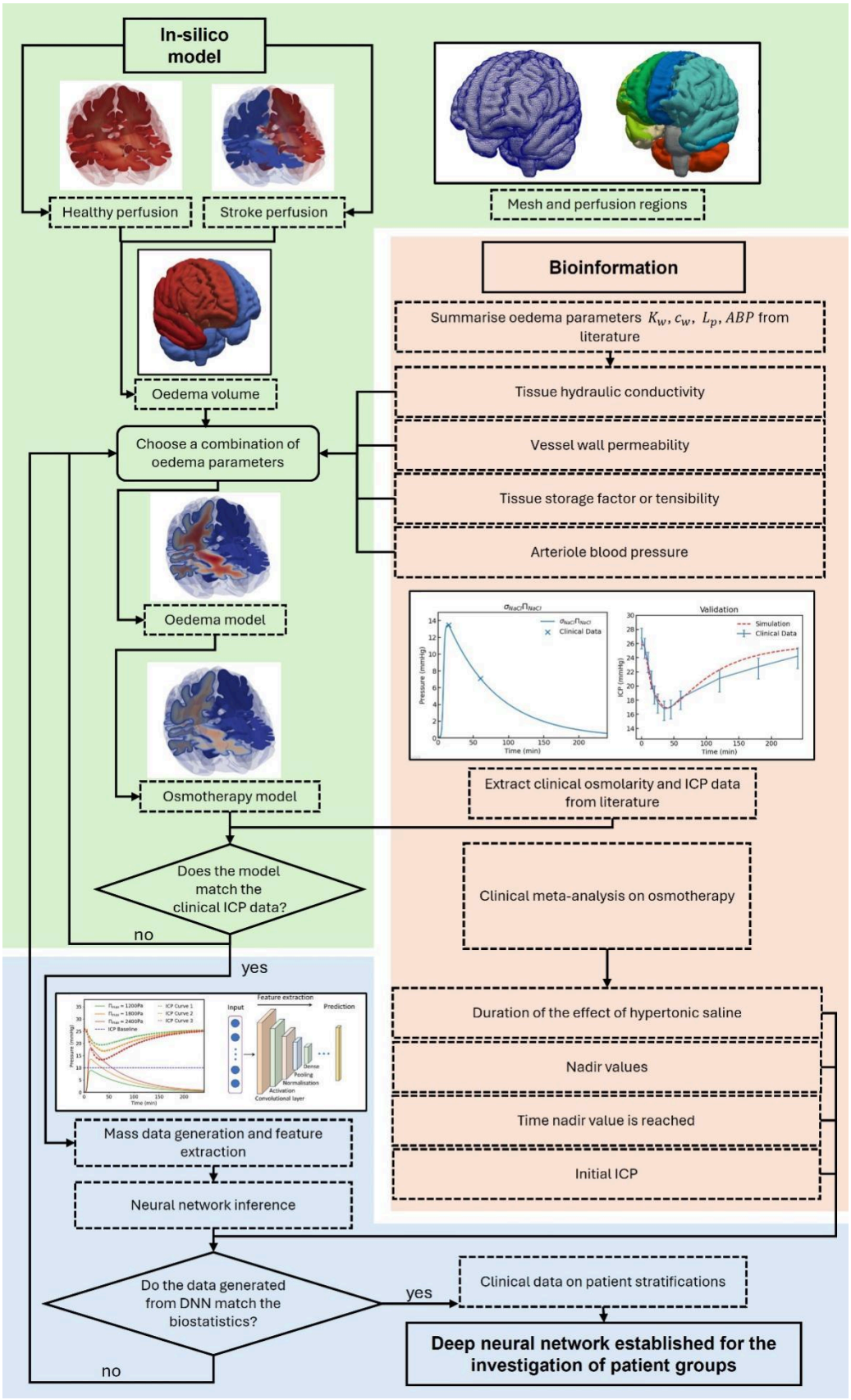

Figure 4: Flowchart illustrating the coupling of the Finite Element method and bioinformatics. The data are used to generate data for deep neural network.

III Results

A. DNN Model Training and ICP Value Estimation

We used a total of 2,000 in silico samples for the DNN model development, out of which we randomly selected 1,600 samples for model training, and the remaining 400 samples were held out for model testing. To obtain a reliable model, we used 10-fold cross-validation to train the DNN model. We divided the whole dataset into training and testing sets, the training data were then randomly split into 10 folds. During each training, 9 of the 10 folds were used for model training and the remaining fold was used for validation. For each iteration, the DNN model was trained for 100 epochs, and the model with the minimal estimation error was stored. The searched optimal model was then used to predict the ICP values in the hold-out testing dataset, which had the performance of 0.249 ± 0.009 mmHg for the error of estimating ICP.

B. Effect of Patient-specific Parameters on ICP Curve Evolution

We first investigate the effects of the physiological parameters on the features of ICP curves over an osmotherapy episode. The parameters vary with patients and are challenging to measure in clinical settings. However, previous studies have indicated a variation of the parameters in different patient groups. For example, the cerebrospinal fluid (CSF) clearance rate in smokers was reported to be lower than in non-smokers, indicating a lower tissue hydraulic conductivity [42]. Meanwhile, the blood vessel leakage was found to be larger in elderly patients, implying a larger value of L_p [43]. In this study, we investigate the effects of different parameters by fixing one of the four parameter inputs and fixing the injection dose input while the rest of the parameters are set to be uniform random variables. The value of the L_p, K_w, or c_w range from 0.5 to 2 times the baseline value and the ABP ranges from 80 mmHg to 100 mmHg. 2000 results are generated for each parameter using the DNN and the initial ICP, nadir ICP, nadir ICP time, and the duration of effect (defined as 10% ICP drop) are plotted as boxplots to show the difference on a simulation quasi-population level (Fig. 5).

The plots show that the L_p and K_w have the most significant effect on the initial ICP, with a mean of 20.8 to 25.6 mmHg and 22.6 to 26.1 mmHg, respectively (Fig. 5g). In contrast, the blood pressure value has only a limited effect on the initial ICP in the range around 22.8 to 24.7 mmHg. As to the nadir ICP values, it is noted that in both 1800 and 3600 Pa maximum osmotic pressure cases, the K_w and c_w presents a strong influence on the lowest ICP whilst the effects of the L_p become less significant compared to its impact on initial pressure (Fig. 5a&d). Similarly, the ABP only shows a slight influence on the lowest pressure. Meanwhile, the time point nadir values are reached are most dependent on L_p and c_w, with a range from 20-115 min. The effect of osmotherapy lasts from 135 to more than 240 min.

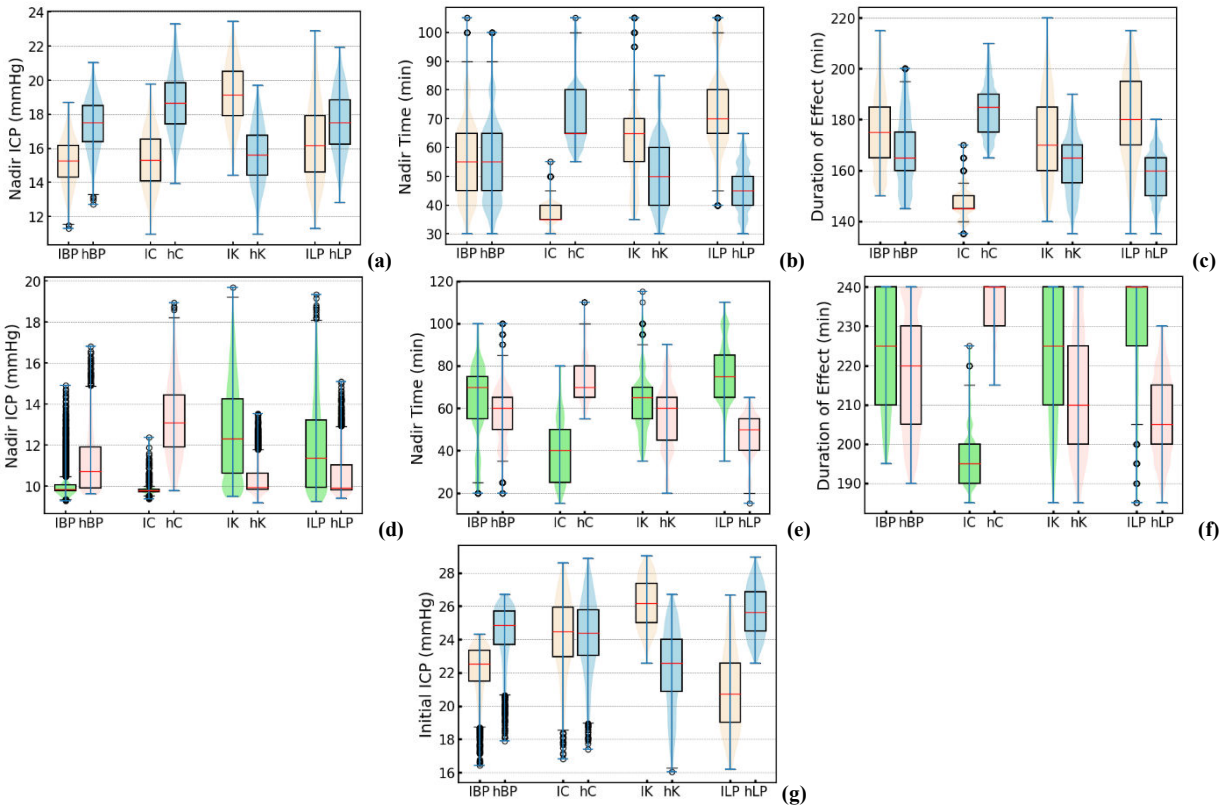

Figure 5: The features of the ICP curve as the flow parameters change. The first row shows the case where dose of injection leads to a maximum osmotic pressure of 1800 Pa, whereas the second row represents the case where maximum osmotic pressure is 3600 Pa. The third row shows

the initial ICP. IBP, hBP denote 80 mmHg and 100 mmHg arteriole blood pressure, respectively. Meanwhile, the lC, hC, lK, hK, lLp, hLp represents 0.5 and 2 times the baseline values of the physiological parameters, with "l" for 0.5 and "h" for 2 times respectively.

C. Evaluation of the Osmotherapy over an Episode Based on Two Criteria

Apart from the effects of the parameters on the ICP curves, the estimation of the effectiveness of osmotherapy is critical in designing a proper treatment plan for different patients. The evaluation of the effectiveness of osmotherapy has been limited by the difficulty in measuring ICP. In some studies, the evaluation is done via measuring the ICP nadir value or the ICP at certain time during an episode. For example, a 10% ICP drop 10 minutes after the end of infusion has been used to determine a successful therapy [30]. Alternatively, the pupillary diameter has also been used to estimate the drop in ICP [44]. Here, two criteria are utilised to estimate the effectiveness of the episode in the model. As the major goal of osmotherapy is to reduce ICP below 20 mmHg, the duration of time of the ICP below 20 mmHg in an episode is divided by the duration of the episode to obtain a time ratio and to indicate how effectively the ICP is reduced below this critical threshold. In addition, the overall pressure drop is divided by the overall rise in the osmotic pressure in the blood during an episode of 240 min to obtain the treatment efficiency, as shown in Equation 11:

$$\mathrm{E_{Mean}} = \frac{\int_0^{240}(\mathrm{ICP}_{t=0} - \mathrm{ICP}) \cdot \mathrm{d}t}{\int_0^{240} \sigma_{NaCl}\Pi_{NaCl} \cdot \mathrm{d}t}. \quad (11)$$

In Fig. 6, the maximum osmotic pressure here is chosen to be 1800 Pa. Virtual patient groups are generated, and 2000 episodes outcome are predicted in each group. To avoid cases with initial pressures below 20 mmHg, only those virtual patients with initial ICP over 25 mmHg are selected. The L_p influences both the efficiency and time ratio by around 15%, whereas the arteriole blood pressure shows a minor effect on efficiency but a significant impact on time ratio by 25%. Meanwhile, the storage factor and K_w affect the time ratio by about 17% and 16%, respectively.

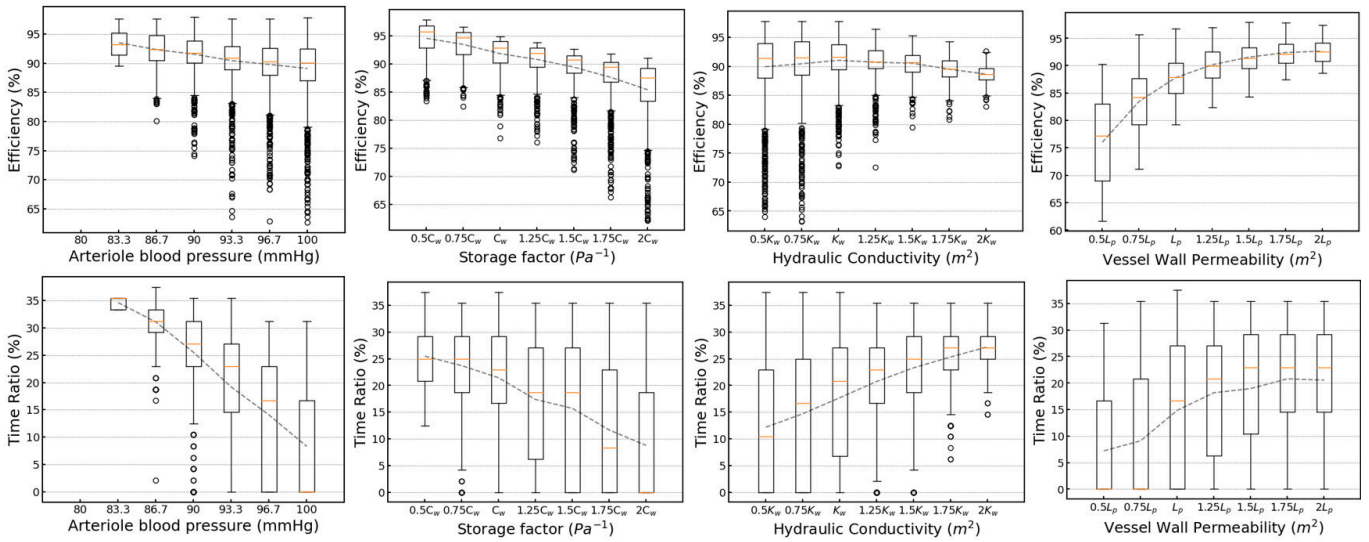

Figure 6: The treatment efficiency and the time ratio of ICP below 20 mmHg of an osmotherapy episode (240 min), where arteriole blood pressure (ABP) shows the blood pressure increment from baseline value of 80 mmHg, c_w is the storage factor, K is the tissue hydraulic conductivity and L_p the vessel wall permeability. The ABP's baseline value is 80 mmHg with a uniform increment to the maximum of 100 mmHg. The boxplots show the median and outliers in the quasi-population level trial and the dotted lines shows the average values of the different groups.

D. The Optimization of Medication Doses for Various Brain Damage Levels

In clinical settings, the physiological parameters vary in different patient groups, especially the vessel wall permeability, which has been shown in the previous section to affect the therapy significantly. The post-stroke damage to the blood-brain barrier can vary depending on whether the treatment is successful. It is also determined by the timing of clinical treatment and the collateral score of the patients [45].

To investigate the optimal treatment of patients with different BBB damage levels, L_p values is varied while the rest of parameters are uniformly random. 2000 virtual patients are generated for each L_p. Similarly, to exclude patients with initial ICP lower than 20 mmHg, only the cases with initial ICP values over 25 mmHg are included (with a fraction of around 5%, 25%, 50%, 62% for $0.5L_p, L_p, 1.5L_p, 2L_p$, respectively).

In Fig. 7a, the efficiency of treatment rises with the L_p, from a mean of around 71.2±9.8% to 93.3±6.8%. Meanwhile, the distributions of time ratio in the patient groups show similar patterns. To investigate the proper dosage for the patient groups, bar charts for the patient number who had ineffective osmotherapy are shown. Fig. 7b&c present the number of patients who had time ratio of 0 and time ratio below 25%, respectively. Here, zero time ratio means that 20 mmHg is not achieved, and below 25% time ratio means 20

mmHg is achieved less than an hour. Overall, an osmotic pressure of 2000 Pa helps reach an ICP below 20 mmHg and 2500 Pa ensures that most patients are treated effectively.

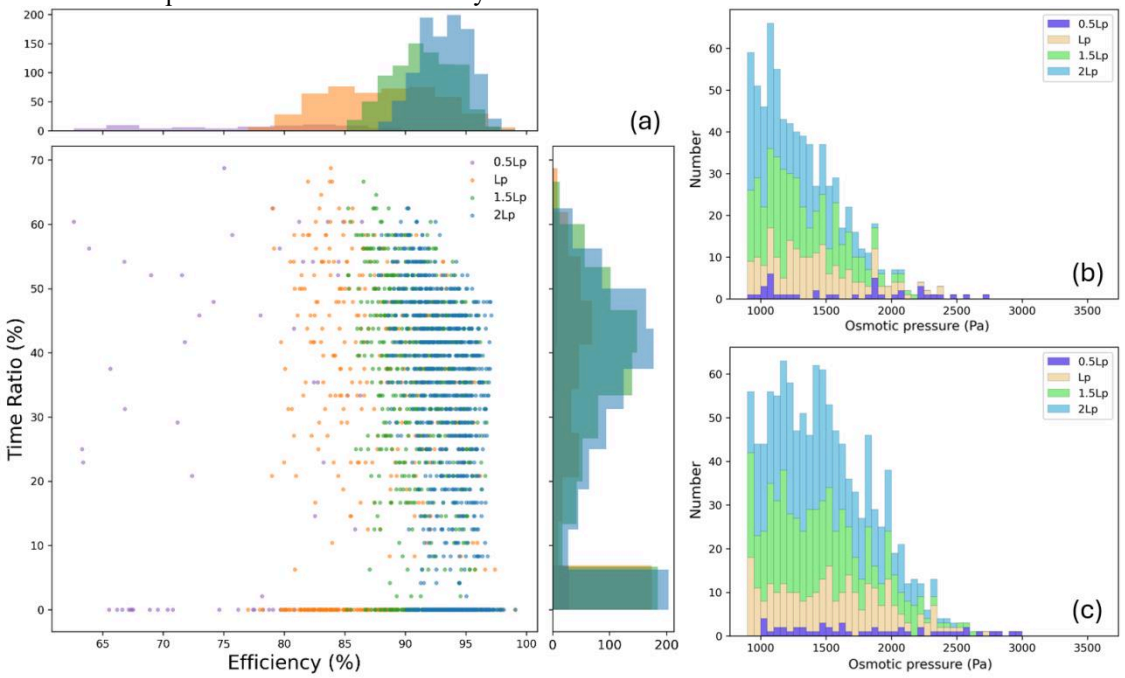

Figure 7: (a) The efficiency and time ratio under different L_p values (0.5, 1, 1.5, 2 times the baseline) and doses of osmotic agent at each injection. (b) Patients are categorised by the maximum osmotic pressure to show patient number with zero time ratio. (c) Patients are categorised by the maximum osmotic pressure to show patient number with below 25% time ratio.

E. The Optimization of Drug Doses for Various Age Groups

Here, we attempt to relate the model parameters with certain patient groups. In clinical settings, the age of patients is an important factor to consider as ageing changes not just the biomedical conditions of the patient but also the mechanical properties of the human brain. According to previous studies, ageing is related to a softening of brain tissue [31, 46], increased blood vessel leakage [43, 47], a decrease in water content in the brain [48-50], a decrease in tissue conductivity [48]. These indicate a lower tissue hydraulic conductivity, a higher vessel leakage rate, larger storage factor in the elder patients. Meanwhile, the mean arterial pressure (MAP) is not found to be statistically different between young and elderly patients [51]. The previous studies on these parameters are summarised in Table B1.

Although there is a decrease in water content in the brain tissue and a reduced hydraulic conductivity in rats, quantitative studies on human brain tissue hydraulic conductivity are rare. In [52, 53], a decrease in the CSF production rate (around half CSF production rate in individuals in their 70s compared to the 30s), whilst CSF production rate is found not age-dependent but rather individual-dependent in a more recent study [54]. It is therefore inferred from the data [52-54] that individuals in their 50s has 1.5 the hydraulic conductivity compared to the 90s as a result of the CSF production rate decrease in the elderly's brains. Meanwhile, the tension test of the brain tissue shows a doubled tension shear modulus in the 50s subjects compared to the 90s subjects [31] and there has been shown a water content decrease with ageing [50]. This indicates a larger storage factor in the 50s. Additionally, 1.5 times the blood vessel wall permeability is implemented to reflect the 1.5 times difference in vessel wall leakage between the 50s and 90s populations [43], whereas the arteriole blood pressure at the pial surface is considered an approximation to mean arterial pressure (MAP).

To investigate the effects of ageing, patients between 50 to 90 years old are studied and 2000 virtual patients are generated for each group. The vessel wall permeability is given a random number between 0.5-1.33 the baseline value for the 50 years group, and these randomly generated values are multiplied 1.5 to represent the 90 years group. The storage factor is 0.5-1 baseline value in the 50s and doubled in the 90s. Tissue hydraulic conductivity is given a random number between 0.5-1.33 the baseline value in the 90s and 0.75-2 in the 50s age group. In the meantime, the arteriole blood pressure values are generated randomly between 80 to 100 mmHg for both age groups. The efficiency and time ratio for the evaluation of osmotherapy episodes are shown in Fig. 8. In the results, it can be seen that the 90s has a more than three times incidence of developing oedema beyond 25 mmHg (Fig. 8a). The efficiency and time ratio of the 50s and 90s age group are similar, with a higher risk of ineffective (20 mmHg not achieved) in the 90s. meanwhile, Fig. 8b&c show that 1500-2000 Pa osmotic pressure is needed to effectively treat the 50 s, whereas 2000-2500 Pa is needed for the 90s. Finally, Fig. 8d shows the probability of the time ratio of the 90s treated with different doses. It is found that a dosage that creates osmotic pressure of 1500 Pa and below can be ineffective in

most cases, but the effectiveness can rise significantly beyond a certain threshold (around 2100 Pa).

IV. Discussion

To the best of our knowledge, this study presents the first osmotherapy in silico trial assisted by a DNN. In clinical se-

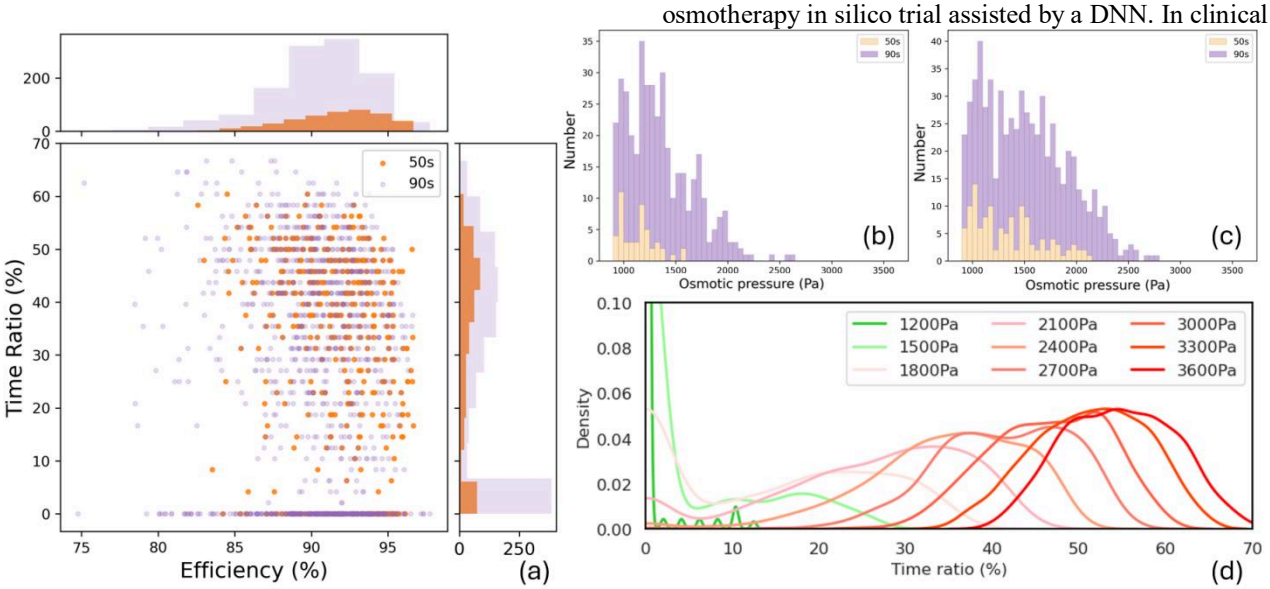

Figure 8: (a) The efficiency and time ratio of the 50s and the 90s age groups. (b) Patients are categorised by the maximum osmotic pressure to show patient number with zero time ratio. (c) Patients are categorised by the maximum osmotic pressure to show patient number with below 25% time ratio. (d) Probability density function of the time ratio for the 90s under various maximum osmotic pressure.

-ttings, the treatment of brain oedema is usually based on the medical history and other characteristics of the patients, for example, the ages, sex, etc. These patient data have been widely used to predict the outcome and the severity of oedema. However, how the medical history and patient characteristics are correlated with the ICP and with other flow parameters remains unclear. In this study, a DNN is utilised to generate virtual patients and the flow parameters are related to patient groups of various levels of BBB damage and ages. 2000 patients are used for each patient group throughout the study to eliminate the effects of randomness and obtain reliable results. Here, the DNN can generate data 10^8 faster than the FE model and provide flexibility in the choice of physiological parameters. Therefore, the DNN is trained for the investigation of osmotherapy in various patient stratifications and utilised as the surrogate of the validated FE model to generate large dataset. To our knowledge, this is the first attempt to correlate the clinical statistics to a FE mathematical model. This helps tackle the challenge in osmotherapy studies as the ICP data can be rare in clinical settings. More importantly, this study bridges the gap between bioinformatics and biophysical laws by providing an osmotherapy model that is supported by both well-founded mathematical/mechanical theories and patient data.

As shown in Fig. 4, the model parameters are chosen from [2, 31-36] and is validated with both the clinical curves from [30] and bioinformation from previous literature [55-58] to determine the best combination of model parameters. The model generates simulation results that are in good match with the clinical data when compared with 8 oedema patients (average ages of 59.8±8.8) who underwent 22 episodes using 10% hypertonic saline (Fig. 2e). In section 3.2, the simulation results show that the initial ICP ranges from around 16 to 29 mmHg, which agrees well with the clinical ICP rise to [15, 30] mmHg [4]. Meanwhile, the effect of hypertonic saline on ICP lasts more than 2 hours in the model, the mean of maximum ICP drop 9.72 mmHg, and nadir values are reached between 15-115 min after the therapy. This matches excellently with clinical studies, where the mean maximum ICP reduction is 10.1 [55] and 11.4 mmHg [56, 57], the nadir values are achieved at 15-120 min [55, 56, 58], and the ICP usually remain decreased 1-5+ hours after infusion [8, 58]. Furthermore, the cases with 3600 Pa maximum osmotic pressure (20% hypertonic saline) generates a pressure drop of around 54.3% from initial ICP (Fig. 5), which agrees well with the retrospective studies [44, 59], where a 55.6% and around 50% pressure drop was found in 23.4% hypertonic saline treatment. Generally, the ICP curves generated from the study can match the clinical data in terms of the nadir, initial ICP values and the time these critical values are reached. It therefore guarantees that the in silico trials are comparable to clinical data.

However, previous clinical studies mostly focus on the doses and types of osmotic agents and there is no existing study on patient stratification. This is because ICP measurement involves high risks and the patient samples are usually small. This makes it impossible to further stratify the patients in clinical studies. Here, in silico trials can be a nice complementary tool to investigate osmotherapy in different patient groups. As it is important to optimise the injection dose in clinical settings to control the side-effects of treatment [11–13], we thus present the first in silico trial investigation of treatment strategy in various patient stratifications. In the DNN predicted results, the initial ICP mainly depends on the L_p and the hydraulic conductivity. In contrast, the effect of arteriole blood pressure is not as significant as a variation of ABP from 80 to 100 mmHg only leads to an around 2 mmHg difference in the initial ICP in the virtual patients. This indicates that fluid accumulation is highly dependent on the

restriction of the blood-brain barrier on the fluid flow through the vessel wall. Meanwhile, the lowest ICP is strongly affected by the choice of storage factor (Fig. 5). As brain tissue with a small storage factor can respond to the osmotic pressure rise in the blood vessel in a shorter period of time, brains with a small storage factor also experience a faster pressure rebound after the osmotic pressure drops as the drug concentration starts dropping. Therefore, the storage factor of the brain tissue has multiple effects on the ICP curve. Interestingly, the virtual patient data show that a smaller storage factor can lead to a lower minimum ICP, larger time ratio and higher efficiency during an episode. This indicates that a small storage factor (saturated brain) is favourable to osmotherapy.

Furthermore, the AI-assisted in silico trial is evaluated based on two criteria, the time ratio, and the efficiency. The model is used to study different patient groups, including patients with various levels of BBB damage and patients at different ages, namely the 50s and the 90s age group populations. In the patient groups with different L_p values, the efficiency varies whilst the time ratio shows a similar pattern among these groups. Differing from our previous study on osmotherapy [26], where the dose of the medication shows a strong influence on specific cases, only patient groups are considered in Fig. 7b&c. It is challenging to obtain the exact value of the parameters and it is therefore reasonable to consider an optimization on a population-averaged level. In Fig. 7b&c, the virtual patients show a 2000-2500 Pa osmotic pressure is sufficient to achieve ICP below 20 mmHg in most cases. Considering the side effects and the marginal ICP drop, higher doses are thus not proposed unless radical treatment is needed in clinical settings. The failure of osmotherapy can be caused by drug insensitivity or the low dose of injection [11]. This investigation shows that a dose of 10% (1800 Pa) can induce sufficient ICP drop in most of the population (Fig. 7&8) and therefore other types of osmotic agents are suggested if the treatment is ineffective when 10% hypertonic saline has been used.

The simulation results present a higher possibility of osmotherapy failure in the 90s population and the virtual patient groups show that a larger dose is needed for the elderly (90s) population to guarantee an ICP below 20 mmHg (Fig. 8). Furthermore, the density plot of time ratio in the 90s show a threshold in the effectiveness in osmotherapy (Fig. 8d). Therefore, a failure in osmotherapy can have multiple reasons: ineffectiveness when using small doses below the threshold; and insensitivity of patients to certain types of osmotic agents [2, 30]. Therefore, the dosage needs to be sufficiently improved before another osmotic agent or other therapeutic strategies are considered.

Finally, the DNN model provides fast inference of ICP curves and therefore is a tool for more in-time clinical decision-making. DNN also provides more flexibility compared to FE simulations and has the potential to incorporate multi-modal data compared to traditional FEM. The current model is only trained by biomechanical parameters. Once there are more clinical data and improved understanding of more complex biochemical and physiological factors, it can incorporate more patient characteristics, such as age, sex and medical history for better prediction of optimised treatment strategy.

Limitations

This study has several limitations. Firstly, the multi-compartment model comprises many model parameters and determining the accurate values of all of the parameters is highly challenging. Due to the limited experimental data, there lacks comparison between the parameter values in different studies. As far as we know, [32, 33] are the only study on the tissue hydraulic conductivity conducted by one group. The tissue hydraulic conductivity value is thus chosen from the range of experimental data in [32, 33]. However, such value can depend on the experimental methods and brain tissue samples used, and therefore can be further examined when more experimental data become available in parallel studies. Secondly, the parameters including K_w, c_w and L_p data for different age groups are not yet available in the oedema brains and experimental data from healthy brains are used [31, 43, 52-54]. The risks of in-vivo measurements of ICP also make the existing ICP clinical data very rare and these clinical studies are limited to only severe cases of brain oedema. Thirdly, only normalised blood flow is considered in the FE model after stroke treatment. In clinical settings, there can be reduced blood flow due to vessel collapse and clot fragmentation [60, 61], and increased blood flow caused by hypertension after reperfusion [62]. There still lacks a full mathematical description of these phenomena and this can make the modelling of oedema more complicated. According to previous studies, however, the effects of vessel collapse and clot fragmentation are usually local [60] and hyperperfusion is the less common compared to normalised blood flow [62, 63]. We thus consider the idealised scenario of a normalised blood flow in the FE model is reasonable. A further developed model that includes these scenarios will require a better mathematical description of the blood flow regulation and local occlusions. Furthermore, variations of brain geometry are neglected as this study focuses on the pressure evolution during osmotherapy. The deformation has been shown to be a fast time scale variation compared to pressure change in oedema and thus has limited impact on ICP evolution [29]. However, the treatment of oedema can also involve brain surgeries such as craniectomy and this will require further future development of the model for the simulation of brain tissue deformation. Finally, the model only takes into account the difference in the brain mechanical properties among patient groups. Other factors such as biochemistry and pathology are not considered here.

V. Conclusions

In conclusion, this is the first study combining the conventional FE model with AI methods to investigate osmotherapy on a quasi-population level to the authors' knowledge. The model bridges the gap between biophysical laws and bioinformatics to provide a novel approach to studies various patient groups in osmotherapy. Once more accurate mechanical properties and physiological parameters of the brain become available. The model will be able to

provide a more accurate prediction of clinical outcomes and thus improve the clinical treatment of brain oedema.

APPENDIX

Appendix A: Parameter Value Ranges

The experimental data from the previous studies are summarised in Table A1:

TABLE A1:
EXPERIMENTAL DATA AND THEIR SOURCES FOR PATIENTS IN 50S AND 90S.

Physiological Parameters		
Arteriole blood pressure [51]	95±11 mmHg in the 50s	98±11 mmHg in the 90s
Tension shear modulus [31]	Around 500 Pa in the 50s	Around 250 Pa in the 90s
CSF production rate [52]	0.41±0.24 in the 30s	0.19±0.07 in the 80s
Vessel wall leakage rate [43]	7.5 min^{-1} in the 50s	12 min^{-1} in the 90s

An around two times difference are shown in L_p and tension shear modulus between the 50s and 90s groups. Although the vessel leakage rate is measure in healthy brains, the value is simply taken to be around 1.5 times in oedema patients as there is not yet any relevant dataset.

Appendix B: Model Parameters

TABLE B1:
MODEL PARAMETERS.

Parameter Values			
c_b	1.59×10^{-3} Pa^{-1}	R_c	5×10^{-6} m
c_w	3.08×10^{-4} Pa^{-1}	σ	0.35
K_a	1.234 $mm^3 s \cdot kg^{-1}$	σ_{NaCl}	0.062
K_c	4.28×10^{-3} $mm^3 s \cdot kg^{-1}$	Π_c	2445 Pa
K_v	2.468 $mm^3 s\ kg^{-1}$	ω_{ac}^{g}	1.326×10^{-6} $Pa^{-1}s^{-1}$
K_w	3.6×10^{-3} $mm^3 s\ kg^{-1}$	ω_{ac}^{w}	5.22×10^{-7} $Pa^{-1}s^{-1}$
L_p	3.0×10^{-11} m/s·Pa	ω_{cv}^{w}	4.641×10^{-6} $Pa^{-1}s^{-1}$
n_b	0.03	ω_{cv}^{g}	1.828×10^{-6} $Pa^{-1}s^{-1}$

References

[1] W. Han, Y. Song, M. Rocha, and Y. Shi, "Ischemic brain edema: Emerging cellular mechanisms and therapeutic approaches," *Neurobiology of Disease*, vol. 178, p. 106029, Mar. 2023, doi: https://doi.org/10.1016/j.nbd.2023.106029.

[2] A. M. Cook *et al.*, "Guidelines for the Acute Treatment of Cerebral Edema in Neurocritical Care Patients," *Neurocritical Care*, vol. 32, no. 3, pp. 647–666, May 2020, doi: 10.1007/s12028-020-00959-7.

[3] P. Solar, M. Hendrych, M. Barak, H. Valekova, M. Hermanova, and R. Jancalek, "Blood-Brain Barrier Alterations and Edema Formation in Different Brain Mass Lesions," *Frontiers in Cellular Neuroscience*, vol. 16, Jul. 2022, doi: https://doi.org/10.3389/fncel.2022.922181.

[4] R. J. Hood, D. J. Beard, D. D. McLeod, L. A. Murtha, and N. Spratt, "Intracranial pressure elevation post-stroke: Mechanisms and consequences," *Frontiers in Stroke,* vol. 2, Feb. 2023, doi: 10.3389/fstro.2023.1119120.

[5] A. S. Wahdan, A. A. Al-Madawi, K. A. El-Shafey, and S. H. Othman, "Comparison of intermittent versus continuous infusion of 3% hypertonic saline on intracranial pressure in traumatic brain injury using ultrasound assessment of optic nerve sheath," *Egyptian Journal of Anaesthesia*, vol. 38, no. 1, pp. 291–299, May 2022, doi: https://doi.org/10.1080/11101849.2022.2077052.

[6] M. Mekonnen et al., "Hypertonic Saline Treatment in Traumatic Brain Injury: A Systematic Review," *World Neurosurgery*, Mar. 2022, doi: https://doi.org/10.1016/j.wneu.2022.03.056

[7] D. Holden *et al.*, "Hypertonic saline use in neurocritical care for treating cerebral edema: A review of optimal formulation, dosing, safety, administration and storage," *American Journal of Health-System Pharmacy*, vol. 80, no. 6, pp. 331–342, Dec. 2022, doi: 10.1093/ajhp/zxac368.

[8] J. A. Kølsen-Petersen, "Osmotherapy," in Springer eBooks, 2020, pp. 293–302. doi: 10.1007/978-3-642-28126-6_54.

[9] A. Bernini et al., "Hypertonic lactate for the treatment of intracranial hypertension in patients with acute brain injury," *Scientific Reports*, vol. 12, no. 1, Feb. 2022, doi: https://doi.org/10.1038/s41598-022-07129-z O.

[10] Huet et al., "Impact of continuous hypertonic (NaCl 20%) saline solution on renal outcomes after traumatic brain injury (TBI): a post hoc analysis of the COBI trial," *Critical Care*, vol. 27, no. 1, Jan. 2023, doi: https://doi.org/10.1186/s13054-023-04311-1.

[11] N. Carney et al., "Guidelines for the Management of Severe Traumatic Brain Injury, Fourth Edition," *Neurosurgery*, vol. 80, no. 1, pp. 6–15, Sep. 2016, doi: 10.1227/neu.0000000000001432.

[12] H. S. Mangat, "Hypertonic saline infusion for treating intracranial hypertension after severe traumatic brain injury," *Critical Care*, vol. 22, no. 1, Feb. 2018, doi: 10.1186/s13054-018-1963-7.

[13] J. Gu, H. Huang, Y. Huang, H. Sun, and H. Xu, "Hypertonic saline or mannitol for treating elevated intracranial pressure in traumatic brain injury: a meta-analysis of randomized controlled trials," *Neurosurgical Review*, vol. 42, no. 2, pp. 499–509, Jun. 2018, doi: 10.1007/s10143-018-0991-8.

[14] P. Konduri, H. A. Marquering, E. VanBavel, A. G. Hoekstra, C. B. L. M. Majoie, and I. Investigators, "In silico trials for treatment of acute ischemic stroke," *Frontiers in Neurology*, vol. 11, Sep. 2020, doi: 10.3389/fneur.2020.558125.

[15] C. Miller et al., "In silico trials for treatment of acute ischemic stroke: Design and implementation," *Computers in Biology and Medicine*, vol. 137, p. 104802, Oct. 2021, doi: 10.1016/j.compbiomed.2021.104802.

[16] J. C. Vardakis, L. Guo, D. Chou, and Y. Ventikos, "Using multicompartmental poroelasticity to explore brain biomechanics and cerebral diseases," in *Notes on numerical fluid mechanics and multidisciplinary design*, 2021, pp. 151–163. doi: 10.1007/978-3-030-55594-8_15.

[17] Z. Li et al., "A computational study of fluid transport characteristics in the brain parenchyma of dementia subtypes," *Journal of Biomechanics*, vol. 159, p. 111803, Oct. 2023, doi: 10.1016/j.jbiomech.2023.111803.

[18] T. I. Jozsa, R. M. Padmos, N. Samuels, W. K. El-Bouri, A. G. Hoekstra, and S. J. Payne, "A porous circulation model of the human brain for in silico clinical trials in ischaemic stroke," *Interface Focus*, vol. 11, no. 1, p. 20190127, Dec. 2020, doi: 10.1098/rsfs.2019.0127.

[19] T. Józsa, R. M. Padmos, W. K. El-Bouri, A. G. Hoekstra, and S. J. Payne, "On the Sensitivity Analysis of Porous Finite Element Models for Cerebral Perfusion Estimation," *Annals of Biomedical Engineering*, vol. 49, no. 12, pp. 3647–3665, Jun. 2021, doi: 10.1007/s10439-021-02808-w.

[20] S. Payne, T. I. Józsa, and W. K. El-Bouri, "Review of in silico models of cerebral blood flow in health and pathology," Prog. Biomed. Eng. (Bristol), vol. 5, no. 2, p. 022003, 2023.

[21] L. Lu et al., "Decoding 2.3 million ECGs: Interpretable Deep learning for advancing cardiovascular diagnosis and mortality risk stratification," *European Heart Journal*, Feb. 2024, doi: 10.1093/ehjdh/ztae014.

[22] L. Lu, Y. Tan, D. Oetomo, I. Mareels, E. Zhao, and S. An, "On model-guided neural networks for system identification". *In IEEE Symposium Series on Computational Intelligence (SSCI)*, 2019, pp. 610-616, doi: 10.1109/SSCI44817.2019.9002703.

[23] Y. Shen, L. Lu, T. Zhu, X. Wang, L. Clifton, Z. Chen, R. Clarke, and D.A. Clifton, "AutoNet-Generated Deep Layer-Wise Convex Networks for ECG Classification". IEEE Transactions on Pattern Analysis and Machine Intelligence, 2024, doi: 10.1109/TPAMI.2024.3378843s.

[24] L. Nie, S. Wu, Z. Wu, and S. Ji, "Efficient generation of pretraining samples for developing a deep learning brain injury model via transfer learning," *Annals of Biomedical Engineering*, Aug. 2023, doi: 10.1007/s10439-023-03354-3.

[25] S. Wu, W. Zhao, and S. Ji, "Real-time dynamic simulation for highly accurate spatiotemporal brain deformation from impact," *Computer Methods in Applied Mechanics and Engineering*, vol. 394, p. 114913, May 2022, doi: 10.1016/j.cma.2022.114913.

[26] X. Chen, T. I. Jozsa, and S. J. Payne, "Computational modelling of cerebral oedema and osmotherapy following ischaemic stroke," *Computers in Biology and Medicine*, vol. 151, p. 106226, Dec. 2022, doi: 10.1016/j.compbiomed.2022.106226.

[27] X. Chen *et al.*, "Mathematical modelling of haemorrhagic transformation in the human brain," *Applied Mathematical Modelling*, vol. 121, pp. 96–110, Sep. 2023, doi: 10.1016/j.apm.2023.04.031.

[28] L. Tatu, T. Moulin, J. Bogousslavsky, and H. M. Duvernoy, "Arterial territories of the human brain," Neurology, vol. 50, no. 6, pp. 1699–1708, Jun. 1998, doi: 10.1212/wnl.50.6.1699.

[29] S. J. Payne, "Interstitial fluid transport in a multi-compartment model of cerebral blood flow," *Journal of Mechanics*, vol. 39, pp. 508–517, Jan. 2023, doi: 10.1093/jom/ufad040.

[30] Š. Schwarz, D. Georgiadis, A. Aschoff, and S. Schwab, "Effects of hypertonic (10%) saline in patients with raised intracranial pressure after stroke," *Stroke*, vol. 33, no. 1, pp. 136–140, Jan. 2002, doi: 10.1161/hs0102.100877.

[31] S. Budday, T. C. Ovaert, G. Holzapfel, P. Steinmann, and E. Kuhl, "Fifty Shades of Brain: A review on the mechanical testing and modeling of brain tissue," *Archives of Computational Methods in Engineering*, vol. 27, no. 4, pp. 1187–1230, Jul. 2019, doi: 10.1007/s11831-019-09352-w.

[32] A. Jamal *et al.*, "Infusion mechanisms in brain white matter and their dependence on microstructure: an experimental study of hydraulic permeability," *IEEE Transactions on Biomedical Engineering*, vol. 68, no. 4, pp. 1229–1237, Apr. 2021, doi: 10.1109/tbme.2020.3024117.

[33] M. Vidotto, D. Botnariuc, E. De Momi, and D. Dini, "A computational fluid dynamics approach to determine white matter permeability," *Biomechanics and Modeling in Mechanobiology*, vol. 18, no. 4, pp. 1111–1122, Feb. 2019, doi: 10.1007/s10237-019-01131-7.

[34] F. Arba et al., "Blood–brain barrier leakage and hemorrhagic transformation: The Reperfusion Injury in Ischemic StroKe (RISK) study," European Journal of Neurology, vol. 28, no. 9, pp. 3147–3154, Jul. 2021, doi: 10.1111/ene.14985.

[35] P. J. Blanco, L. O. Müller, and J. D. Spence, "Blood pressure gradients in cerebral arteries: a clue to pathogenesis of cerebral small vessel disease," *Stroke and Vascular Neurology*, vol. 2, no. 3, pp. 108–117, Jun. 2017, doi: 10.1136/svn-2017-000087.

[36] N. Freeman and J. Welbourne, "Osmotherapy: science and evidence-based practice," *BJA Education*, vol. 18, no. 9, pp. 284–290, Sep. 2018, doi: 10.1016/j.bjae.2018.05.005.

[37] F. Liu et al., "A medical multimodal large language model for future pandemics," Npj Digital Medicine, vol. 6, no. 1, Dec. 2023, doi: 10.1038/s41746-023-00952-2.

[38] M. Kollovieh, A. F. Ansari, M. Bohlke-Schneider, J. Zschiegner, H. Wang, and Y. Wang, "Predict, Refine, Synthesize: Self-Guiding diffusion models for probabilistic time series forecasting," arXiv (Cornell University), Jul. 2023, doi: 10.48550/arxiv.2307.11494.

[39] B. C. V. Campbell *et al.*, "Endovascular Therapy for Ischemic Stroke with Perfusion-Imaging Selection," *The New England Journal of Medicine*, vol. 372, no. 11, pp. 1009–1018, Mar. 2015, doi: 10.1056/nejmoa1414792.

[40] T. Jovin *et al.*, "Diffusion-weighted imaging or computerized tomography perfusion assessment with clinical mismatch in the triage of wake up and late presenting strokes undergoing neurointervention with Trevo (DAWN) trial methods," *International Journal of Stroke*, vol. 12, no. 6, pp. 641–652, Jun. 2017, doi: 10.1177/1747493017710341.

[41] A. Logg, K. Mardal, and G. N. Wells, *Automated solution of differential equations by the finite element Method: the FENICS Book*. 2012. [Online]. Available: http://ci.nii.ac.jp/ncid/BB08773951

[42] L. Guo, J. C. Vardakis, D. Chou, and Y. Ventikos, "A multiple-network poroelastic model for biological systems and application to subject-specific modelling of cerebral fluid transport," *International Journal of Engineering Science*, vol. 147, p. 103204, Feb. 2020, doi: 10.1016/j.ijengsci.2019.103204.

[43] I. C. M. Verheggen *et al.*, "Increase in blood–brain barrier leakage in healthy, older adults," *GeroScience*, vol. 42, no. 4, pp. 1183–1193, Jun. 2020, doi: 10.1007/s11357-020-00211-2.

[44] C. Lazaridis, R. Neyens, J. Bodle, and S. M. DeSantis, "High-Osmolarity saline in neurocritical care," *Critical Care Medicine*, vol. 41, no. 5, pp. 1353–1360, May 2013, doi: 10.1097/ccm.0b013e31827ca4b3.

[45] P. Konduri *et al.*, "Risk factors of late lesion growth after acute ischemic stroke treatment," *Frontiers in Neurology*, vol. 13, Oct. 2022, doi: 10.3389/fneur.2022.977608.

[46] L. V. Hiscox, H. Schwarb, M. McGarry, and C. L. Johnson, "Aging brain mechanics: Progress and promise of magnetic resonance elastography," *NeuroImage*, vol. 232, p. 117889, May 2021, doi: 10.1016/j.neuroimage.2021.117889.

[47] A. Farrall and J. M. Wardlaw, "Blood brain barrier: ageing and microvascular disease-systematic review and meta-analysis," *Journal of the Neurological Sciences*, vol. 283, no. 1–2, p. 261, Aug. 2009, doi: 10.1016/j.jns.2009.02.089.

[48] A. Gottschalk, S. Scafidi, and T. J. K. Toung, "Brain water as a function of age and weight in normal rats," *PLOS ONE*, vol. 16, no. 9, p. e0249384, Sep. 2021, doi: 10.1371/journal.pone.0249384.

[49] M. K. Rasmussen and H. Mestre, "Fluid transport in the brain," *Physiological Reviews*, vol. 102, no. 2, pp. 1025–1151, Apr. 2022, doi: 10.1152/physrev.00031.2020.

[50] R. Gracien *et al.*, "Evaluation of brain ageing: a quantitative longitudinal MRI study over 7 years," *European Radiology*, vol. 27, no. 4, pp. 1568–1576, Jul. 2016, doi: 10.1007/s00330-016-4485-1.

[51] E. Yetim, J. Jacoby, N. L. Damestani, A. Lovely, D. H. Salat, and M. R. Juttukonda, "Mean arterial pressure and cerebral hemodynamics across the lifespan: a Cross-Sectional study from Human Connectome Project-Aging," *Journal of Magnetic Resonance Imaging*, vol. 58, no. 6, pp. 1892–1900, Apr. 2023, doi: 10.1002/jmri.28722.

[52] C. May, J. Kaye, J. Atack, M. B. Schapiro, R. P. Friedland, and S. I. Rapoport, "Cerebrospinal fluid production is reduced in healthy aging," *Neurology*, vol. 40, no. 3_part_1, p. 500, Mar. 1990, doi: 10.1212/wnl.40.3_part_1.500.

[53] R. A. Fishman, "The cerebrospinal fluid production rate is reduced in dementia of the Alzheimer's type," *Neurology*, vol. 58, no. 12, p. 1866, Jun. 2002, doi: 10.1212/wnl.58.12.1866.

[54] P. Gideon, C. Thomsen, F. Ståhlberg, and O. Henriksen, "Cerebrospinal fluid production and dynamics in normal aging: a MRI phase-mapping study," *Acta Neurologica Scandinavica*, vol. 89, no. 5, pp. 362–366, Jan. 2009, doi: 10.1111/j.1600-0404.1994.tb02647.x.

[55] J. J. Belfer, A. V. Patel, R. M. Darracott, D. M. Jackson, J. D. Nordeen, and W. D. Freeman, "Safety and efficacy of repeated doses of 14.6 or 23.4 % hypertonic saline for refractory intracranial hypertension," *Neurocritical Care*, vol. 20, no. 3, pp. 436–442, Sep. 2013, doi: 10.1007/s12028-013-9907-1.

[56] R. Nau, "Osmotherapy for elevated intracranial pressure," Clinical Pharmacokinetics, vol. 38, no. 1, pp. 23–40, Jan. 2000. doi:10.2165/00003088-200038010-00002

[57] L. L. Forsyth, X. Liu-DeRyke, D. Parker, and D. H. Rhoney, "Role of hypertonic saline for the management of intracranial hypertension after stroke and traumatic brain injury," Pharmacotherapy: The Journal of Human Pharmacology and Drug Therapy, vol. 28, no. 4, pp. 469–484, Apr. 2008. doi:10.1592/phco.28.4.469

[58] A. Torre-Healy, N. F. Marko, and R. J. Weil, "Hyperosmolar therapy for intracranial hypertension," *Neurocritical Care*, vol. 17, no. 1, pp. 117–130, Nov. 2011, doi: 10.1007/s12028-011-9649-x.

[59] A. J. Kerwin, M. A. Schinco, J. J. Tepas, W. H. Renfro, E. Vitarbo, and M. Mühlberger, "The use of 23.4% hypertonic saline for the management of elevated intracranial pressure in patients with severe traumatic brain injury: a pilot study," *Journal of Trauma-injury Infection and Critical Care*, vol. 67, no. 2, pp. 277–282, Aug. 2009, doi: 10.1097/ta.0b013e3181acc726.

[60] A. Ames 3rd, R. L. Wright, M. Kowada, J. M. Thurston, and G. Majno, "Cerebral ischemia. II. The no-reflow phenomenon," Am. J. Pathol., vol. 52, no. 2, pp. 437–453, 1968.

[61] J.-Y. Chueh, A. S. Puri, A. K. Wakhloo, and M. J. Gounis, "Risk of distal embolization with stent retriever thrombectomy and ADAPT," Journal of Neurointerventional Surgery, vol. 8, no. 2, pp. 197–202, Dec. 2014, doi: 10.1136/neurintsurg-2014-011491.

[62] M. Kneihsl et al., "Post-reperfusion hyperperfusion after endovascular stroke treatment: a prospective comparative study of TCD versus MRI,"

Journal of NeuroInterventional Surgery, vol. 15, no. 10, pp. 983–988, Sep. 2022, doi: 10.1136/jnis-2022-019213.
[63] K. Shimonaga et al., “Hyperperfusion after Endovascular Reperfusion Therapy for Acute Ischemic Stroke,” Journal of Stroke and Cerebrovascular Diseases, vol. 28, no. 5, pp. 1212–1218, May 2019, doi: 10.1016/j.jstrokecerebrovasdis.2019.01.007.

https://dspace.org/

AI-assisted in silico trial for the optimization of osmotherapy after ischaemic stroke

Chen, Xi; Lu, Lei; Józsa, Tamás I.; Zhou, Jiandong; Clifton, David A. ...

2025-07-01
Institute of Electrical and Electronics Engineers (IEEE)
https://doi.org/10.1109/jbhi.2025.3541004
Chen X, Lu L, Józsa TI, et al., (2025) AI-assisted in silico trial for the optimization of osmotherapy after ischaemic stroke. IEEE Journal of Biomedical and Health Informatics, Volume 29, Issue 7, July 2025, pp. 5291-5302

Downloaded from a DSpace repository. https://dspace.org/